# Multi-omics elucidation of KDM5C, KDM6A, and KMT2B roles in cancer epigenetic dysregulation and transcriptional reprogramming

Check for updates

Tengjiao Li[1,2,3], Lichen Wang[1,2,3], Shoufeng Duan[1,2], Xinyu Cui[1,2], Chunqing Fu[1,2], Jinglei Hu[1,2] & Lin Li [1,2] ✉

Histone-modifying enzymes (HMEs) are critical regulators of tumorigenesis through epigenetic reprogramming. While mutations in HMEs are recognized drivers of cancer epigenome dysregulation, systematic comparative analyses of their mutational impacts and functional divergence across malignancies remain underexplored. Here, we investigated three HMEs frequently mutated in diverse cancers: KMT2B (H3K4me3 methyltransferase), KDM5C (H3K4me3 demethylase), and KDM6A (H3K27me3 demethylase). Using CRISPR/Cas9-engineered HEK293T knockout cell lines, we performed integrated multi-omics profiling that combined genome-wide chromatin accessibility, transcriptomics, and chromatin-bound proteomics. Contrary to expectations that KMT2B loss (H3K4me3 depletion) and KDM5C loss (H3K4me3 accumulation) would induce opposing transcriptional programs, or that KDM6A deficiency (H3K27me3 accumulation) would exhibit distinct regulatory effects, our analyses revealed distinct effect of all three HME modulations in terms of both transcriptional output and chromatin-associated proteomic state. Functionally, KDM5C loss upregulated FOXF2 and downregulated KLF5, implicating the dysregulation of G protein–coupled receptor pathways; KDM6A loss upregulated JUNB and downregulated TP73, affecting extracellular matrix regulation; and KMT2B loss upregulated JUN and downregulated HOXA10, impacting on cytokine signaling. Notably, transcription factors such as PATZ1 and GATA2 were commonly altered across knockouts. In PANC-1 pancreatic cancer cells, we further confirmed that KDM6A regulates CDH family genes controlling cell adhesion, thereby promoting migration and invasion. Finally, integrative analyzes demonstrated strong correlations between promoter accessibility, transcription factor occupancy, and gene expression, and uncovered cooperation between epigenetic and genetic drivers. Together, these findings reveal context-dependent functional hierarchies among HMEs and underscore the necessity of multi-layered analyses to resolve the complexity of epigenetic regulation in cancer.

Epigenetic dysregulation, particularly aberrant histone methylation, is a hallmark of cancer[1–4]. Histone post-translational modifications (PTMs) dynamically regulate chromatin architecture and transcriptional programs, where site-specific methylation acts as a binary switch for gene activation or repression[1,5,6]. For example, H3K4me1 marks active enhancers, H3K4me3 is enriched at promoter[7–9]. H3K27me3 enforces Polycomb-mediated silencing to preserve cellular identity[10–12]. Bivalent domains carrying both H3K4me3 and H3K27me3 further maintain developmental plasticity in pluripotent and adult stem cells[13,14]. Cancer cells exploit this plasticity by reshaping chromatin landscapes through global DNA hypomethylation, focal

[1]Shanghai Frontiers Science Center of Drug Target Identification and Delivery, Shanghai Key Laboratory for Antibody-Drug Conjugates with Innovative Target, School of Pharmaceutical Sciences, Shanghai Jiao Tong University, Shanghai, China. [2]State Key Laboratory of Innovative Immunotherapy, Shanghai Jiao Tong University, Shanghai, China. [3]These authors contributed equally: Tengjiao Li, Lichen Wang. ✉e-mail: linli@sjtu.edu.cn

hypermethylation, and redistribution of histone marks[2,15,16]. The therapeutic relevance of histone-modifying enzymes (HMEs) is highlighted by pre-clinical successes such as EZH2 inhibition, yet their functional interplay in cancer remains poorly resolved [4,17–19].

A paradoxical feature of cancer epigenetics is the recurrent mutation of functionally opposing HMEs. For instance, both KMT2B (H3K4me3 methyltransferase) and KDM5C (its demethylase) are mutated in >10% of squamous carcinomas, while KDM6A (H3K27me3 demethylase) is altered in >25% of urothelial cancers[20–22]. These coexisting alterations suggest oncogenic mechanisms beyond canonical histone mark homeostasis. Indeed, HME mutations can exert lineage-specific and sometimes para-doxical effects—for example, KDM5C loss can upregulate tumor sup-pressors, whereas KMT2B loss may either promote or block differentiation. Such variability implies that HMEs act within broader transcription factor (TF)–driven circuits, but the identity and hierarchy of these networks remain elusive.

Multi-omics integration offers a powerful framework to address this complexity by linking chromatin accessibility, transcriptional states, and proteomic interactions into unified regulatory maps[23,24]. Landmark studies have applied this paradigm to breast, oral, and pan-cancer cohorts, revealing enhancer activation, chromatin reorganization, and cancer-specific reg-ulatory drivers[25,26]. Yet, most efforts focus on single HMEs or heterogeneous patient cohorts, leaving unresolved how distinct HME mutations compar-ably reshape chromatin states and transcriptional programs in controlled, isogenic settings. Systematic, head-to-head analyzes are essential to disen-tangle context-dependent functions of HMEs and to reveal mechanistic vulnerabilities that may be exploited therapeutically.

To systematically investigate how distinct histone-modifying enzymes (HMEs) coordinate transcriptional regulation in oncogenesis, we generated isogenic CRISPR/Cas9 knockout lines of HEK293T cells targeting KDM5C, KDM6A, and KMT2B. This experimental paradigm enables comparative multi-omics profiling (ATAC-seq, chromatin-bound proteomics, and transcriptomics) under controlled genetic backgrounds, circumventing confounding intercellular heterogeneity. Our integrative analysis reveals three fundamental insights. It shows that each HME governs unique chromatin accessibility patterns at promoters and enhancers that extend beyond canonical histone mark deposition/removal. Meanwhile, chromatin proteomics revealed distinct sets of transcription factors (TFs) recruited by each HME, implicating enzyme-specific mechanisms for chromatin reor-ganization. These findings establish a paradigm for decoding context-specific epigenetic regulation while providing mechanistic insights into cancer-associated chromatin remodeling processes.

## Results

### KDM5C, KDM6A and KMT2B show high mutation frequency in different tumors

KDM5C, KDM6A, and KMT2B exhibit frequent genetic alterations across diverse human malignancies, as evidenced by their inclusion among the top 20 most frequently mutated genes in specific cancer types (Fig. 1a and Supplementary Fig. 1a, b)[27,28]. The majority of these mutations are char-acterized as truncating or missense variants, strongly suggesting functional inactivation (Supplementary Fig. 1c). Analysis of expression patterns in mutated samples reveals distinct trends: demethylases KDM5C and KDM6A demonstrate prominent downregulation across most cancer types, while the methyltransferase KMT2B shows upregulation in various malignancies (Fig. 1b–d and Supplementary Fig. 2a–c), which is consistent with their high mutations in cancer tissues as shown in Fig. 1a. Notably, these enzymes also serve as prognostic biomarkers in multiple cancer contexts. For instance, reduced expression of KDM5C and KDM6A correlates with adverse survival outcomes in Bladder Urothelial Carcinoma (BLCA) patients from The Cancer Genome Atlas (TCGA) cohort, whereas elevated KMT2B expression predicts poor prognosis in Adrenocortical Carcinoma (ACC) (Supplemen-tary Fig. 3a–c). These findings collectively implicate KDM5C, KDM6A, and KMT2B as critical regulators of tumorigenesis, with their dysregulation potentially driving distinct oncogenic processes through opposing expression

dynamics. The observed mutational patterns and prognostic associations underscore the need for further mechanistic investigation into their roles in chromatin remodeling and cancer progression.

### CRISPR-mediated depletion of KDM5C, KDM6A, and KMT2B alters histone modifications and drives phenotypic reprogram-ming in cells

To elucidate the functional contributions of KDM5C, KDM6A, and KMT2B to tumorigenesis, we employed CRISPR/Cas9 genome-editing technology to generate knockout (KO) cell lines for each gene (Supple-mentary Fig. 4a–c). Specifically, HEK293T cells were chosen as the model system because they display moderate expression of the three HMEs examined, making them well-suited for single-gene KO generation and controlled comparison of their epigenetic functions. Given the enzymatic activities of these proteins, we assessed the levels of their corresponding histone modification targets via western blot analysis in the KO cell lines. Consistent with their enzymatic roles, H3K4me3 levels were elevated in KDM5C[KO] cells and reduced in KMT2B[KO] cells, while H3K27me3 levels increased in KDM6A[KO] cells (Fig. 2a–c, Supplementary Fig. 5a–f). Biological phenotypic analysis indicated that ablation of KDM5C, KDM6A, or KMT2B uniformly suppressed cellular proliferation (Fig. 2d–g). However, only KDM6A deficiency enhanced cell migration (Fig. 2h, i), whereas loss of KDM5C or KMT2B had no discernible impact on migratory capacity (Supplementary Fig. 6a, b). Our results indicate that although KDM5C, KDM6A, and KMT2B exert distinct effects on histone methylation, knockout of each enzyme consistently alters cell proliferation, implying their involvement in divergent regulatory mechanisms.

### CRISPR-mediated knockout of KDM5C, KDM6A, and KMT2B induces genome-wide alterations in chromatin accessibility

To investigate the interplay between transcriptomic dysregulation and epi-genetic remodeling induced by the knockout of KDM5C, KDM6A, and KMT2B, we performed Assay for Transposase-Accessible Chromatin using sequencing (ATAC-seq) on the three knockout cell lines to evaluate changes in chromatin accessibility. Ablation of KDM5C resulted in genome-wide alterations in chromatin accessibility at approximately 2029 loci ($|\log_2FC| > 0.263$, FDR < 0.05), with 70% of these significantly altered ATAC-seq peaks exhibiting increased accessibility and 30% showing decreased accessibility (Fig. 3a and Supplementary Data 1). Similarly, KDM6A deficiency led to chromatin accessibility changes at 2,077 sites ($|\log_2FC| > 0.263$, FDR < 0.05), with 27% of peaks displaying increased accessibility and 73% decreased accessibility (Fig. 3b and Supplementary Data 1). Loss of KMT2B induced accessibility changes at 2753 loci ($|\log_2FC| > 0.263$, FDR < 0.05), with 42% of peaks showing increased accessibility and 58% decreased accessibility (Fig. 3c and Supplementary Data 1). The majority of differentially accessible regions were localized to promoters, introns, intergenic regions, and exons (Fig. 3d). Notably, KDM5C depletion enhanced chromatin accessibility at promoter regions, consistent with the observed elevation in H3K4me3 levels in KDM5C[KO] cells (Fig. 3e). Conversely, KMT2B ablation reduced promoter accessibility, mirroring the decrease in H3K4me3 levels in KMT2B[KO] cells (Fig. 3e). KDM6A deficiency decreased accessibility at both promoter and intron regions, reflecting the increased H3K27me3 levels in KDM6A[KO] cells (Fig. 3e). These alterations in chromatin accessibility might indicate changes in chromatin-binding proteins, which subsequently leads to modifications in the transcriptional regulation of downstream genes.

To identify key transcription factors (TFs) driving oncogenic gene expression following KDM5C, KDM6A, or KMT2B loss, we conducted motif analysis on differentially accessible ATAC-seq peaks at promoter regions using MEME Suite (version 5.5.7)[29]. Regions with increased acces-sibility upon KDM5C or KDM6A depletion were enriched for binding motifs of the SP/KLF and STAT transcription factor families (Fig. 4a, b and Supplementary Data 2), which contributed to oncogenesis in previously report[30–32], aligning with the upregulation of cancer-related pathways (Fig. 5f, g). Although regions with increased accessibility upon KDM5C or
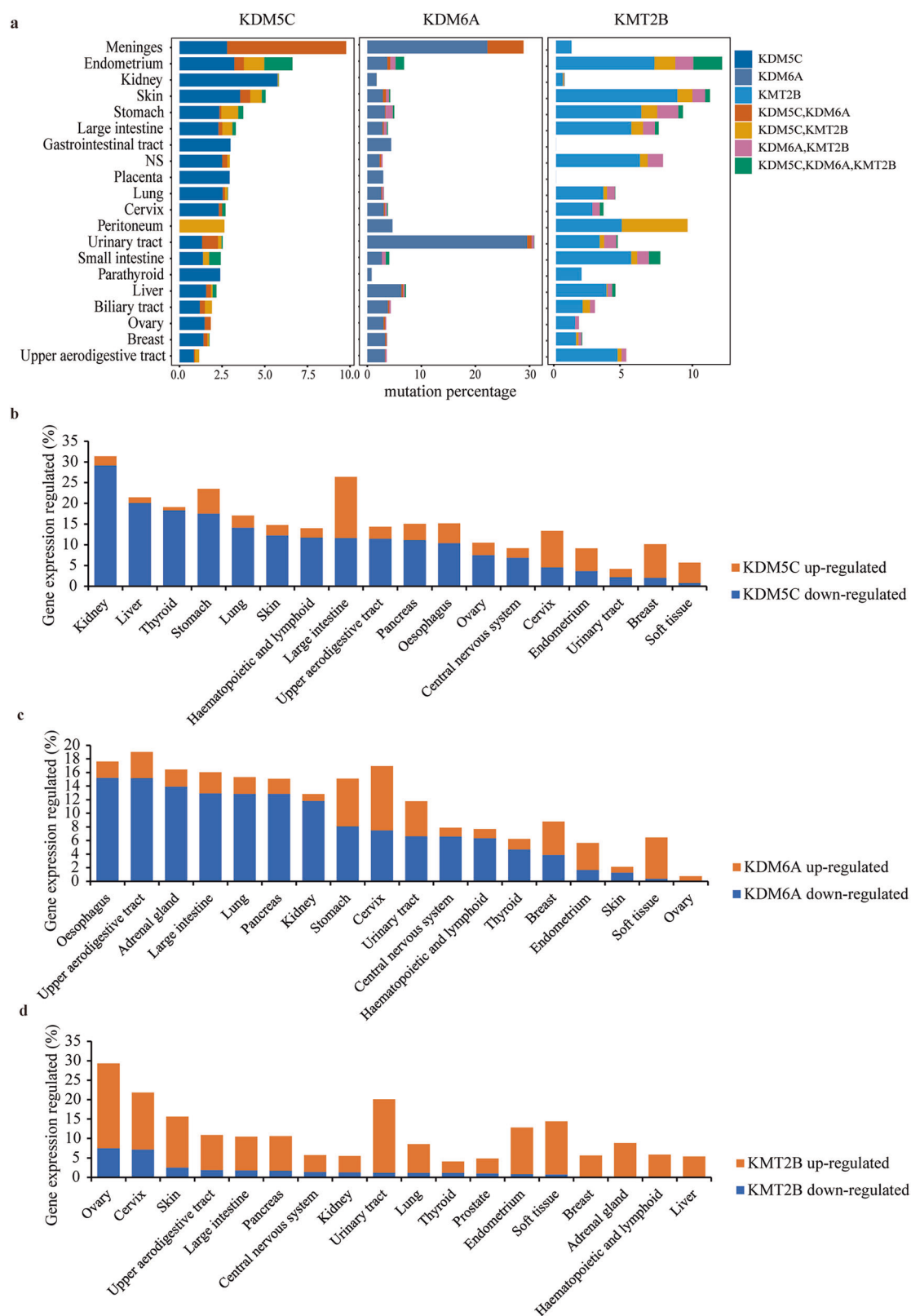
**Fig. 1 | _KDM5C, KDM6A, KMT2B_ are frequently altered genes in various cancer types. a** The mutated frequencies of _KDM5C, KDM6A, KMT2B_ in different human tissue cancer types as described in COSMIC v101. **b–d** Frequency of expression trends of _KDM5C, KDM6A, KMT2B_ in different human tissue cancer types. Data were obtained from the TCGA dataset via cBioPortal.
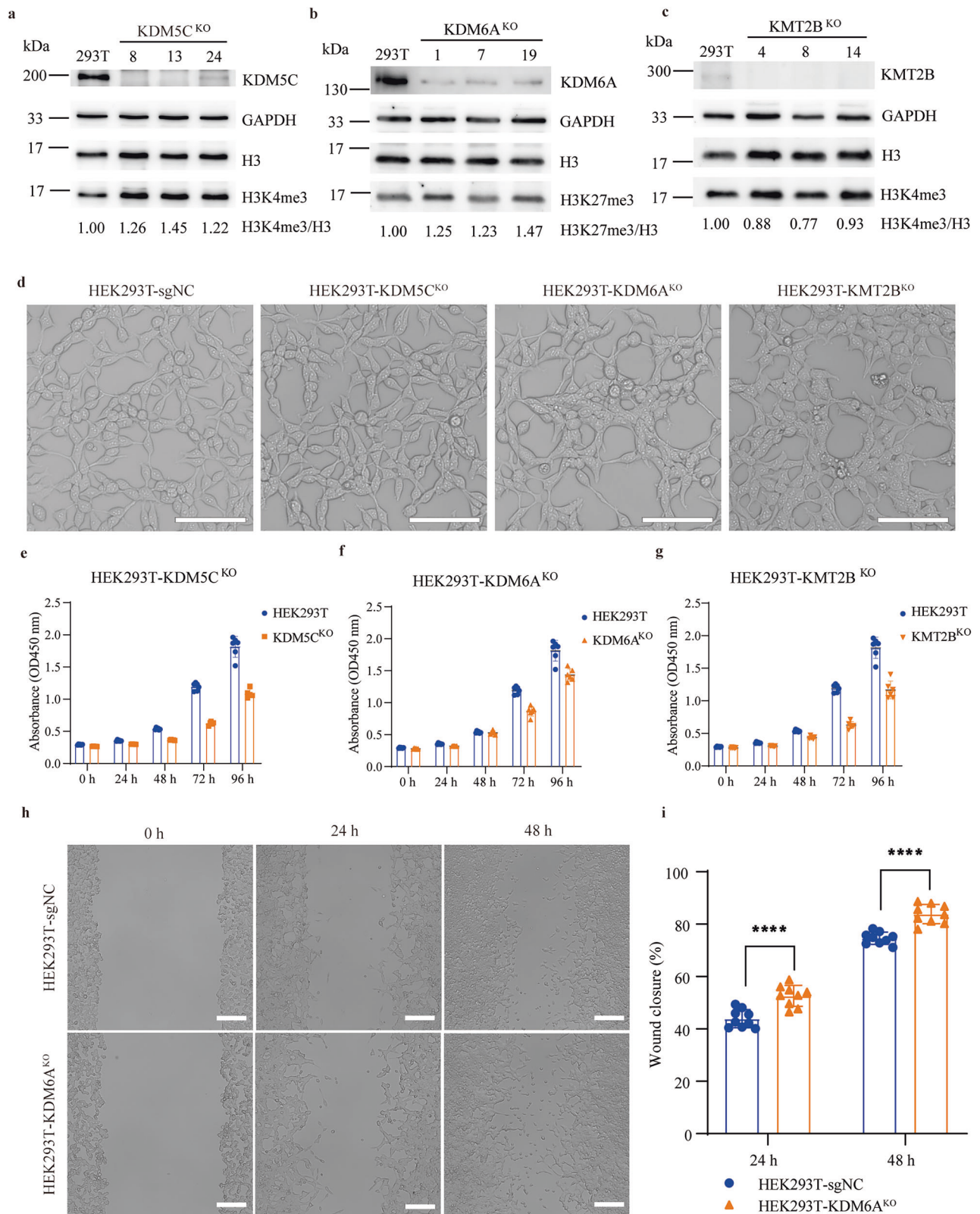
**Fig. 2 | The roles of *KDM5C*, *KDM6A* and *KMT2B* in epigenomic landscape, cell proliferation and migration. a** Immunoblot analyses of KDM5C and H3K4me3 in KDM5C[KO] cells. **b** Immunoblot analyses of KDM6A and H3K27me3 in KDM6A[KO] cells. **c** Immunoblot analyses of KMT2B and H3K4me3 in KMT2B[KO] cells. **d** Representative microscopic images of KDM5C[KO], KDM6A[KO] and KMT2B[KO] cells. Bar: 100 μm. **e–g** Effect of KDM5C, KDM6A and KMT2B knockout on cell proliferation was examined by MTT assays. **h** Representative images and **i** quantification of cell migration of KDM6A[KO] cells. Bar: 200 μm. ****$p < 0.0001$.
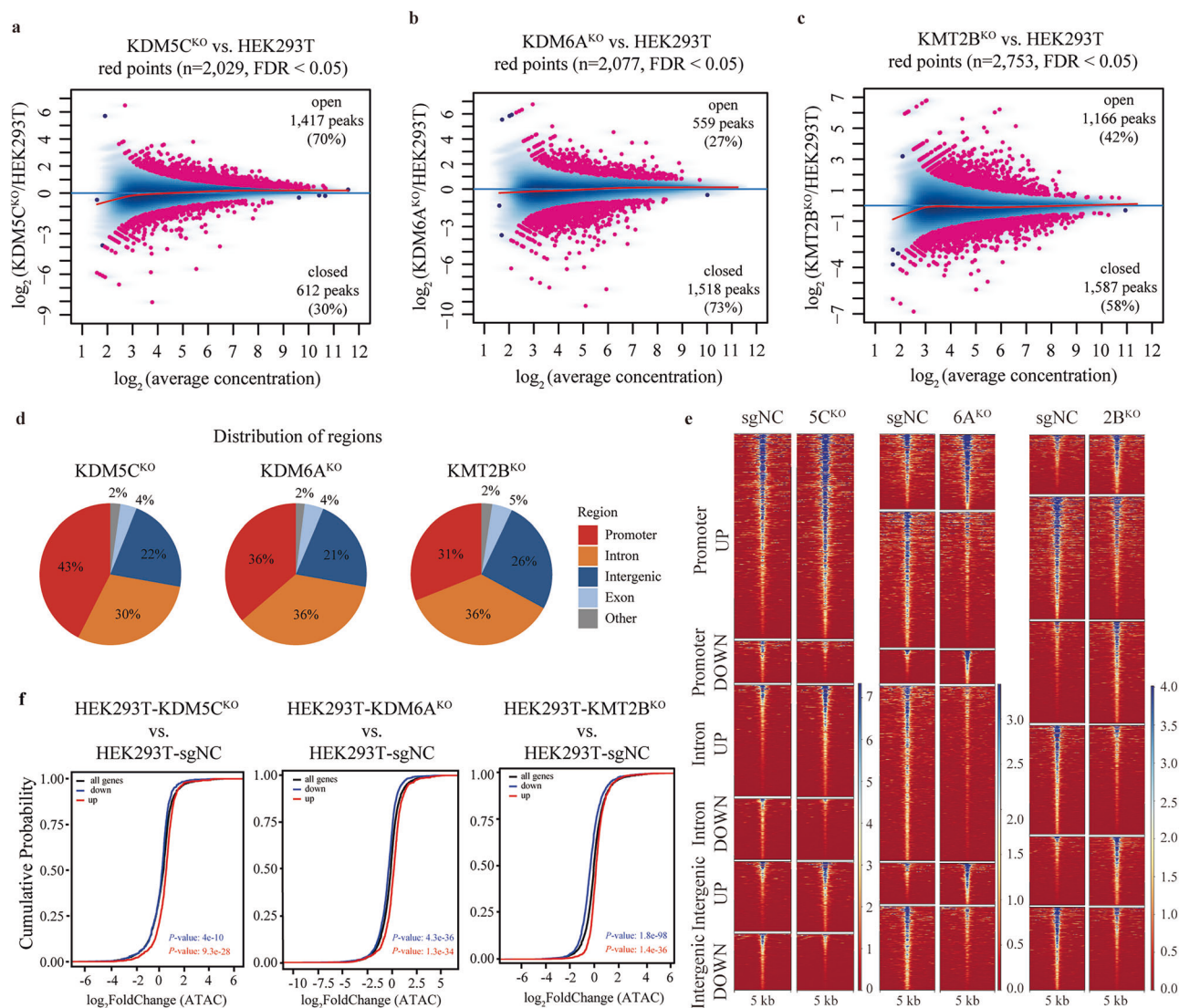
**Fig. 3 | Loss of KDM5C, KDM6A or KMT2B induced a genome-wide changes in chromatin accessibility that correlates with transcriptomic dysregulation.** MA plot of ATAC-seq peaks comparing KDM5C[KO] to WT cells (**a**), KDM6A[KO] to WT cells (**b**), and KMT2B[KO] to WT cells (**c**). The numbers of peaks with significant changes ($|\log_2 FC| > 0.263$, FDR < 0.05, redpoints) were shown. **d** Pie charts showed the percentage of differentially accessible ATAC-seq peaks ($|\log_2 FC| > 0.263$, FDR < 0.05) at promoter, intronic, intergenic and exonic regions. **e** Heat map of differentially accessible ATAC-seq peaks described in a ($|\log_2 FC| > 0.263$, FDR < 0.05) in a 5-kilobase (kb) window grouped by localization at promoter, intron and intergenic regions. **f** Distribution of chromatin accessibility changes associated with significantly upregulated (red) or downregulated (blue) genes comparing KDM5C[KO], KDM6A[KO], KMT2B[KO], with WT cells. $p$ values were calculated using a two-sided Kolmogorov–Smirnov (KS) test comparing peaks associated with differentially expressed genes to all genes.

KDM6A depletion were both enriched for binding motifs of STAT transcription factor families, KDM5C depletion enriched for three STAT transcription factors STAT1, STAT2, STAT3, while KDM6A depletion enriched for only STAT1 and STAT2 and most of these binding motifs were located at the different genes (Supplementary Fig. 7a, b). Whereas, regions altered by KMT2B loss were enriched for SP/KLF and AP1 (JUN/FOS) family TF motifs (Fig. 4c and Supplementary Data 2), consistent with the upregulation of apoptosis-related transcriptional pathway (Fig. 5h). Collectively, these data demonstrate that the loss of KDM5C, KDM6A, or KMT2B induces chromatin accessibility changes that potentiate oncogenic transcriptional programs.

## Chromatin proteome remodeling in KDM5C, KDM6A, and KMT2B knockout cells reveals alterations in chromatin dynamics and transcriptional regulation

Histone post-translational modifications (PTMs) serve as critical regulators of chromatin dynamics by recruiting effector proteins that orchestrate downstream processes such as transcription, recombination, replication, DNA repair, and genomic architecture modulation[33,34]. Dysregulation of these modifications has been implicated as oncogenic drivers[1,6,10,33,35]. Given the genome-wide alterations in chromatin accessibility observed in KDM5C[KO], KDM6A[KO], and KMT2B[KO] cells, particularly through changes in H3K4me3 and H3K27me3 levels, we hypothesized that the loss of these epigenetic modifiers would also induce substantial shifts in the chromatin-binding proteome. To investigate this, we conducted proteomic profiling of chromatin-associated proteins in KDM5C[KO], KDM6A[KO], and KMT2B[KO] cells (Fig. 4d).

In KDM5C[KO] cells, we identified ~4610 chromatin-binding proteins, with 248 proteins showing decreased abundance and 226 exhibiting increased abundance ($|\log_2 FC| > 0.263$, FDR < 0.05) relative to wild-type (WT) cells (Fig. 4e and Supplementary Data 3). Similarly, KDM6A[KO] cells displayed ~4820 chromatin-binding proteins, among which 836 were downregulated and 733 were upregulated ($|\log_2 FC| > 0.263$, FDR < 0.05) (Fig. 4f and Supplementary Data 3). In KMT2B[KO] cells, ~4560 chromatin-
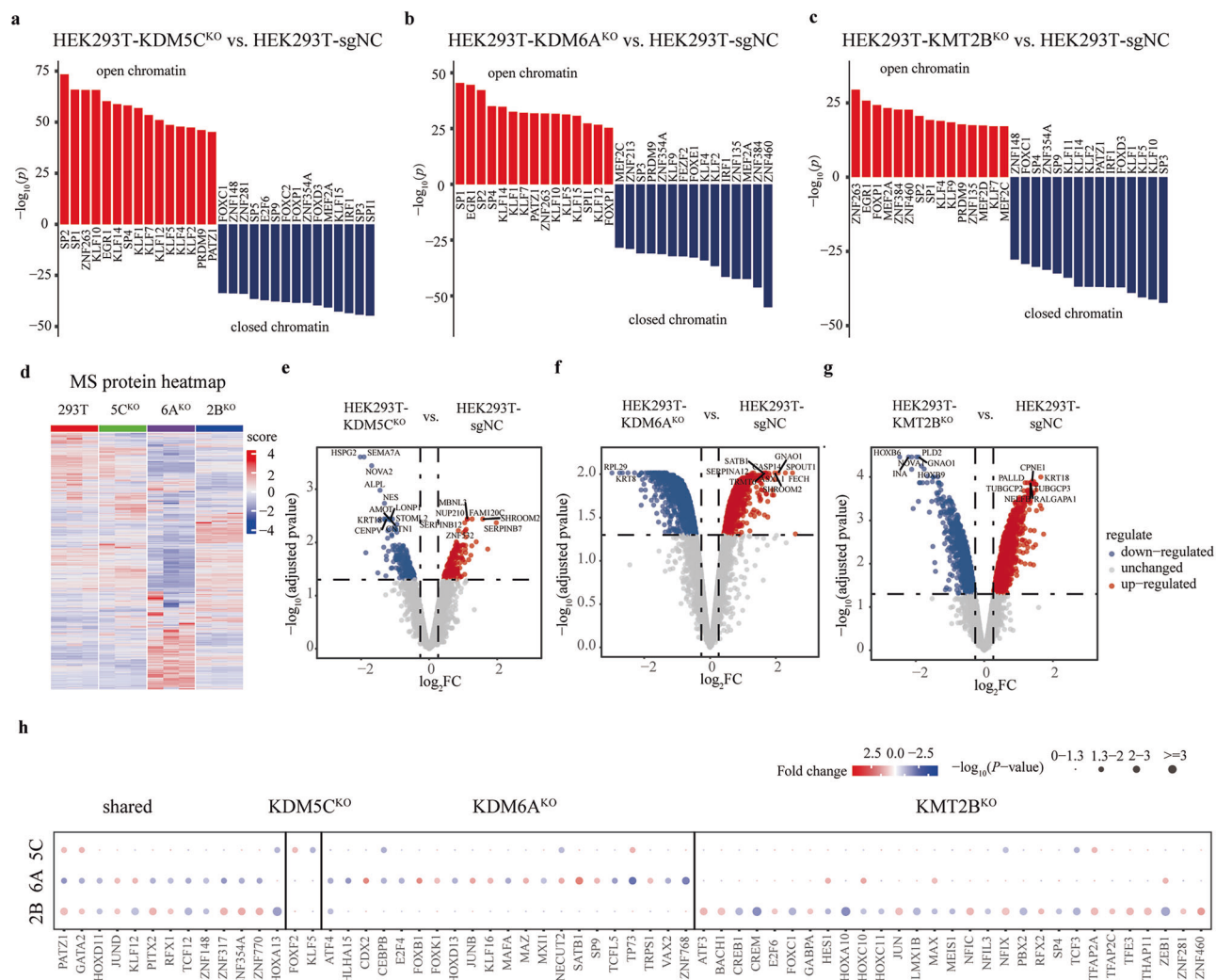
**Fig. 4 | Loss of KDM5C, KDM6A or KMT2B induced genome-wide epigenetic reprogramming by altering the chromatin binding proteome.** The 15 most significantly enriched transcription factor (TF) binding motifs in open (red) and closed (blue) chromatin promoter region peaks comparing **a** KDM5C[KO], **b** KDM6A[KO], and **c** KMT2B[KO] to WT cells. **d** Heatmap of chromatin binding proteome of KDM5C[KO], KDM6A[KO] or KMT2B[KO] cells. Volcano plots of chromatin binding proteome comparing **e** KDM5C[KO], **f** KDM6A[KO], and **g** KMT2B[KO] to WT cells. The chromatin binding proteins with significant changes are highlighted ($|\log_2FC| > 0.263$, FDR < 0.05); red, up-regulated; blue, down-regulated. **h** The TFs with significant changes in both chromatin binding proteome and differentially accessible chromatin regions. The bubble size shows the -$\log_{10}(p$ value) of TFs and the color conveys the fold change of TFs in chromatin binding proteome.

binding proteins were detected, with 848 decreased and 1022 increased proteins compared to WT cells ($|\log_2FC| > 0.263$, FDR < 0.05) (Fig. 4g and Supplementary Data 3). Kyoto Encyclopedia of Genes and Genomes (KEGG) pathway enrichment analysis of the chromatin-bound proteome revealed widespread changes in transcription factors associated with cell cycle regulation, hormone signaling, and infection-related pathways, indicating that depletion of KDM5C, KDM6A, and KMT2B primarily disrupts transcriptional regulation (Supplementary Fig. 8). Collectively, these findings show that loss of KDM5C, KDM6A, and KMT2B induces extensive reprogramming of the chromatin-binding proteome, highlighting their critical roles in maintaining epigenetic and transcriptional homeostasis.

### Transcriptomic dysregulation arising from KDM5C, KDM6A, and KMT2B deficiency

To elucidate the impact of chromatin remodeling on cancer-related signaling pathways, we conducted transcriptomic analyzes of the three knockout (KO) cell lines and identified differentially expressed genes (DEGs) compared to wild-type (WT) cells (Fig. 5a–e and Supplementary Data 4). Notably, KDM5C knockout led to a distinct transcriptomic shift, with 1045 genes

significantly upregulated and 869 genes downregulated ($|\log_2FC| > 0.585$, FDR < 0.05) (Fig. 5c and Supplementary Data 4). This pattern was consistent with the observed elevation in the transcription elongation marker H3K4me3 (Fig. 2a). In contrast, KDM6A knockout resulted in the upregulation of 1119 genes and downregulation of 1317 genes ($|\log_2FC| > 0.585$, FDR < 0.05) (Fig. 5d and Supplementary Data 4), aligning with the increased levels of the transcriptional repressive marker H3K27me3 (Fig. 2b). Meanwhile, KMT2B deficiency induced 1222 upregulated genes and 1365 downregulated genes ($|\log_2FC| > 0.585$, FDR < 0.05) (Fig. 5e and Supplementary Data 4), reflecting the decreased levels of the transcription elongation marker H3K4me3 (Fig. 2c). Gene Set Enrichment Analysis (GSEA) of the RNA-seq data revealed significant enrichment of several cancer-related signaling pathways in the KO cells, including the regulation of response to type II interferon, cell-cell adhesion, and the regulation of endothelial cell apoptotic processes (Fig. 5f–h). Moreover, KMT2B knockout led to compensatory upregulation of several related HMEs, including KDM5A/B/C, KDM6A, and KMT2C/D, at both RNA and chromatin-bound protein levels (Supplementary Fig. 9). Venn analysis of RNA-seq differentially expressed genes (DEGs) across KDM5C, KDM6A, and KMT2B knockouts further revealed a subset of commonly regulated targets (Supplementary Fig. 10),
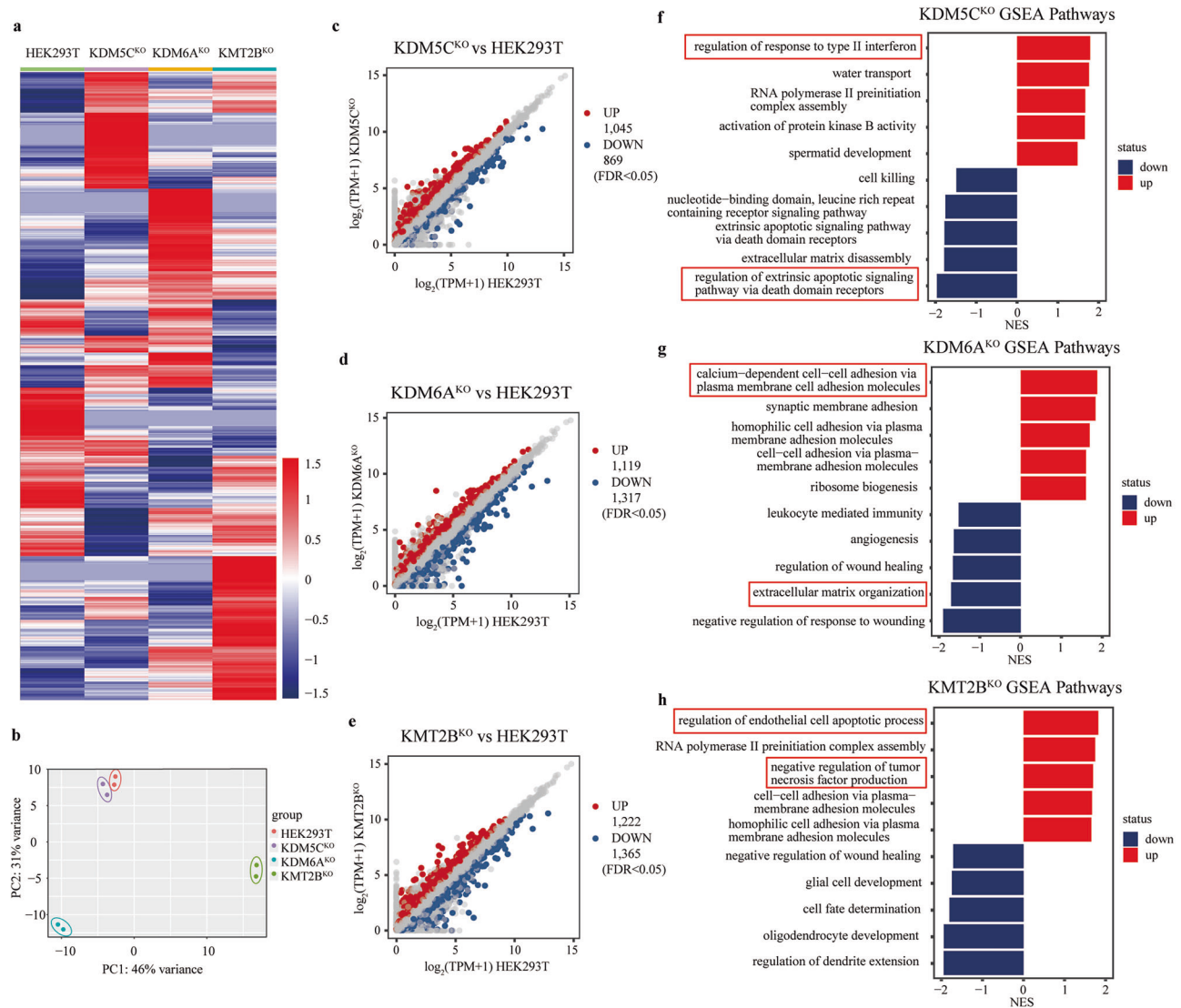
**Fig. 5 | Loss of KDM5C, KDM6A or KMT2B induced transcriptomic dysregulation associated with cancer transition. a** Heatmap and **b** PCA of gene expression data of KDM5C$^{KO}$, KDM6A$^{KO}$ or KMT2B$^{KO}$ cells. **c** A scatter plot comparing the $\log_2$(TPM + 1) values for RNA-seq data in HEK293T cells and KDM5C$^{KO}$ cells. A total of 1045 and 869 transcripts were significantly ($|\log_2$FC$| > 0.585$, FDR < 0.05) up- and downregulated, respectively, in KDM5C$^{KO}$ cells. **d** A scatter plot comparing the $\log_2$(TPM + 1) values for RNA-seq data in HEK293T cells and KDM6A$^{KO}$ cells. A total of 1119 and 1317 transcripts were significantly ($|\log_2$FC$| > 0.585$, FDR < 0.05) up- and downregulated, respectively, in KDM6A$^{KO}$ cells. **e** A scatter plot comparing the $\log_2$(TPM + 1) values for RNA-seq data in HEK293T cells and KMT2B$^{KO}$ cells. A total of 1222 and 1365 transcripts were significantly ($|\log_2$FC$| > 0.585$, FDR < 0.05) up- and downregulated, respectively, in KMT2B$^{KO}$ cells. Bar plot of significantly enriched pathways identified by Gene Set Enrichment Analysis (GSEA) comparing KDM5C$^{KO}$ to WT cells (**f**), KDM6A$^{KO}$ to WT cells (**g**), and KMT2B$^{KO}$ to WT cells (**h**) using the indicated gene sets; NES normalized enrichment score.

suggesting that these enzymes may function in cooperative or partially redundant networks. Such interplay likely contributes to cancer initiation and progression and warrants further investigation.

Collectively, these findings demonstrate that the loss of KDM5C, KDM6A, and KMT2B triggers epigenetic remodeling and transcriptomic dysregulation, thereby promoting oncogenic transformation.

## Oncogenic transcriptional reprograming via chromatin-binding proteome dysregulation in KDM5C, KDM6A, and KMT2B knockout cells

To elucidate the interplay between chromatin accessibility dynamics and transcriptional output, we integrated ATAC-seq data with RNA-seq profiles. Overall, we observed a clear correlation between alterations in chromatin accessibility and gene expression patterns: genes that were upregulated were associated with increased chromatin openness, whereas downregulated genes correlated with chromatin closure (Fig. 3f).

To identify the key TFs that regulate oncogenic transcriptional programs induced by the loss of KDM5C, KDM6A, and KMT2B, we compared TFs predicted from differential chromatin accessibility peaks at promoter regions with differentially expressed proteins identified in the chromatin-binding proteome (Supplementary Fig. 11a–c). In KDM5C$^{KO}$ cells, we identified 3 co-upregulated and 2 co-downregulated TFs; in KDM6A$^{KO}$ cells, 12 co-upregulated and 21 co-downregulated TFs were found; and in KMT2B$^{KO}$ cells, 21 co-upregulated and 20 co-downregulated TFs were observed (Supplementary Fig. 11a–c). The majority of these TFs exhibited cell-type specificity, while a few were common across all three knockout cell lines (Fig. 4h). Examples of cell-specific TFs included FOXF2 and KLF5 in KDM5C$^{KO}$ cells, KLF16, TP73, and JUNB in KDM6A$^{KO}$ cells, and JUN, NFIC, and HOXA10 in KMT2B$^{KO}$ cells. Notably, TFs such as PATZ1 and GATA2 were common across all three knockout cell lines. It is important to highlight that several of these TFs, including members of the JUN and HOX families, TP73, and GATA2, have been implicated in cancer-related processes[36–39].
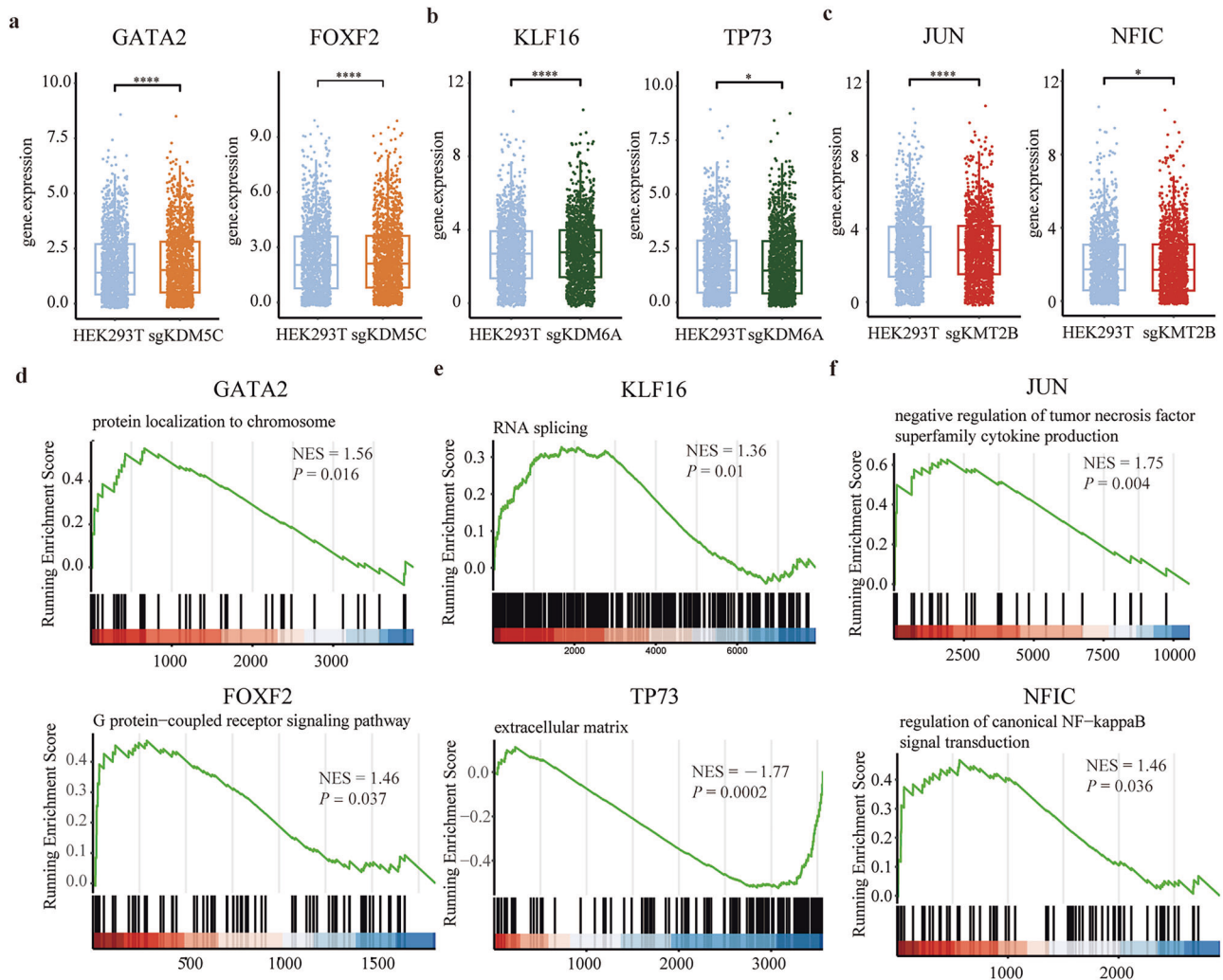
**Fig. 6 | Chromatin binding transcription factor changes in KDM5C$^{KO}$, KDM6A$^{KO}$ or KMT2B$^{KO}$ cells regulated oncogenic transcriptional output.**
**a** Downstream genes of transcription factors (TF) GATA2 and FOXF2 were upregulated at an overall level in KDM5C$^{KO}$ cells. The gene set are the top 1500 of TF target genes. $^*0.01 \le p < 0.05$; $^{****}p < 0.0001$. **b** Downstream genes of KLF16 were upregulated, while downstream genes of TP73 were downregulated at an overall level in KDM6A$^{KO}$ cells. **c** Downstream genes of JUN and NFIC were upregulated at an overall level in KMT2B$^{KO}$ cells. **d** Gene set enrichment analysis (GSEA) plots of GATA2 and FOXF2 target genes comparing KDM5C$^{KO}$ to WT cells. **e** GSEA plots of KLF16 and TP73 target genes comparing KDM6A$^{KO}$ to WT cells. **f** GSEA plots of JUN and NFIC target genes comparing KMT2B$^{KO}$ to WT cells.

To validate the target genes of each TF, we utilized TF-specific chromatin immunoprecipitation followed by sequencing (ChIP-seq) data from the ENCODE project[40] and investigated the regulatory relationships between these TFs and their target genes, referred to as regulons, in KDM5C$^{KO}$, KDM6A$^{KO}$, and KMT2B$^{KO}$ cells. This analysis revealed concordant gene expression patterns between TFs and their targets (Fig. 6a–c), with each analysis encompassing the top 1500 target genes. For instance, compared to WT cells, the target gene sets of the upregulated TF GATA2 exhibited enhanced activity in KDM5C$^{KO}$ cells, while the target gene sets of the downregulated TF TP73 showed decreased activity in KDM6A$^{KO}$ cells, and the target gene sets of the upregulated TF JUN displayed altered activity in KMT2B$^{KO}$ cells (Fig. 6a–c). Additionally, we found that the target genes of knockout-specific regulons were enriched in cancer-specific pathways (Fig. 6d–f), indicating their involvement in oncogenic processes. These results validate the connections among target gene expression, chromatin accessibility, and TF activity.

**KDM6A depletion alters cell adhesion gene expression, enhancing migration and invasion in PANC-1 Cells**
Given that HEK293T-KDM6A$^{KO}$ cells exhibited enhanced cell migration and enrichment of the cell-cell adhesion pathway in Gene Set Enrichment

Analysis (GSEA), we investigated the mRNA levels of several cell adhesion genes. We observed upregulation of CDH2 and CDH12, whereas CDH3 expression was downregulated in KDM6A$^{KO}$ cells (Fig. 7b, c). Correspondingly, the promoter regions of CDH2, and CDH12 displayed increased chromatin accessibility, while the promoter region of CDH3 showed reduced accessibility in KDM6A$^{KO}$ cells (Fig. 7a). These findings align with previous reports indicating that CDH2 and CDH12 act as promoters[41,42], while CDH3 functions as an inhibitor of cell migration[43]. These results suggest that the loss of KDM6A mediates alterations in chromatin accessibility at the promoter regions of cell adhesion genes, thereby enhancing the migratory capacity of KDM6A$^{KO}$ cells.

Pancreatic ductal adenocarcinoma (PDAC) remains one of the most lethal malignancies, with a 5-year survival of less than 11%[44], and recent whole-genome sequencing analysis of PDAC showed frequent mutations in KDM6A (Fig. 1b, e)[45]. We selected the PANC-1 cell line because it retains functional KDM6A, providing a suitable model to generate knockout lines and study its role in this cancer context. To further validate our findings, we silenced KDM6A in pancreatic cancer PANC-1 cells using lentiviral transduction (Supplementary Fig. 12a, b). Subsequently, we assessed the role of KDM6A in pancreatic cancer cell migration and invasion. Wound healing and transwell invasion assays demonstrated that KDM6A
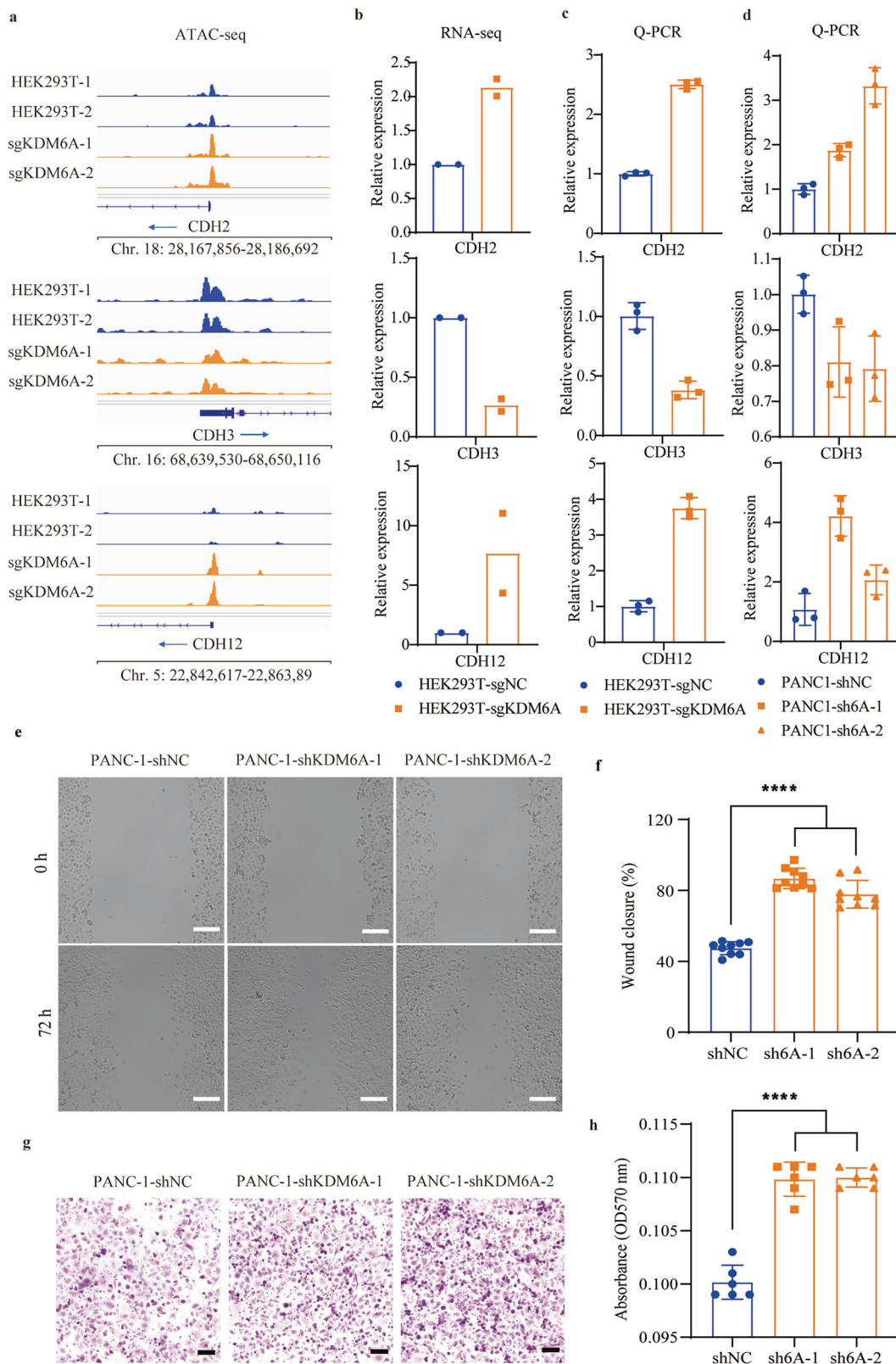
**Fig. 7 | KDM6A loss of function induces the promoter regions accessibility changes of *CDH2*, *CDH3*, and *CDH12* to promote PANC-1 migration and invasion. a** Integrative genomic viewer (IGV) snapshot of accessible chromatin peaks at *CDH2*, *CDH3*, and *CDH12* gene promoter regions in KDM6A^KO and WT cells. **b** Relative expression of *CDH2*, *CDH3*, and *CDH12* genes from RNA-seq data. Relative expression of *CDH2*, *CDH3*, and *CDH12* genes was assessed in **c** HEK293T-KDM6A^KO and **d** PANC-1-shKDM6A cells by real-time fluorescent quantitative PCR (RT–qPCR). **e, f** Representative images and quantifications of migration capability of control and PANC-1-shKDM6A cells by wound healing assay. Bar: 200 μm. **g, h** Representative images and quantifications of invasion capability of control and PANC-1-shKDM6A cells by transwell assay. Bar: 100 μm. ****$p < 0.0001$.

knockdown promoted both migration and invasion capabilities in PANC-1 cells (Fig. 7e–h). Consistently, the expression levels of CDH2, CDH3, and CDH12 were also altered in KDM6A-knockdown PANC-1 cells (Fig. 7d). Collectively, these data indicate that the loss of KDM6A induces changes in the expression of cell adhesion genes, thereby promoting cell migration and invasion.

## Discussion

Classical tumor biology posits that transcriptomic dysregulation is a defining feature of cancer, underpinning critical processes such as uncontrolled proliferation, invasion, and metastasis[15]. Epigenetic modifiers, including KDM5C, KDM6A, and KMT2B, are frequently mutated across diverse cancer types, yet their functional roles in shaping the cancer epigenome and transcriptome remain incompletely understood. In this study, we systematically investigated the consequences of depleting KDM5C, KDM6A, or KMT2B in a unified cellular context, revealing distinct yet interconnected mechanisms by which these enzymes modulate chromatin accessibility, transcription factor (TF) binding dynamics, and oncogenic gene expression programs.

Our findings reveal that depletion of KDM5C, KDM6A, or KMT2B produces distinct but interconnected effects on chromatin and transcription. This is consistent with prior work showing that individual HMEs often act in pathway- and context-specific manners rather than through broad, global shifts in histone methylation. For example, Leng et al. demonstrated that KDM6A cooperates with KMT2B to regulate transcriptional networks in lung cancer[46], while Seehawer et al. uncovered a KDM6A–MMP3 axis driving metastasis upon KMT2C/D loss in breast cancer[47]. Our study extends these findings by showing that, even in isolation, each enzyme directs unique TF networks and cancer-relevant pathways, yet also displays compensatory and overlapping functions, reflected in the upregulation of related HMEs and shared sets of differentially expressed genes.

Importantly, our multi-omic approach highlights the central role of TFs as mediators between chromatin remodeling and oncogenic gene expression. The observation that TFs such as PATZ1 and GATA2 are regulated in opposite directions depending on the HME context underscores both the therapeutic potential and complexity of targeting TF networks. Rather than acting as universal oncogenic or tumor-suppressive switches, their activity is highly context dependent, echoing recent calls for precision epigenetic strategies that take cellular state into account.

Functionally, KDM6A knockdown in PANC-1 cells enhanced migration and invasion, accompanied by dysregulation of cadherin family genes (e.g., CDH2, CDH3, CDH12). Chromatin proteomics revealed marked shifts in TF occupancy upon HME loss, consistent with changes in chromatin accessibility. For instance, SATB1, JUNB, and JUND were upregulated in KDM6A-deficient cells, likely driving CDH2 activation and epithelial–mesenchymal transition[48–50]. These observations highlight how HME perturbations reshape TF binding landscapes, thereby amplifying or attenuating oncogenic transcriptional programs.

In summary, our work provides a comprehensive resource that situates KDM5C, KDM6A, and KMT2B within the broader landscape of epigenetic control of oncogenesis. By defining how these enzymes reshape chromatin accessibility and TF occupancy, we highlight candidate regulatory nodes that may serve as therapeutic entry points. At the same time, the observed context dependence cautions against simplistic targeting strategies and underscores the need for further in vivo and disease-specific studies to translate these mechanistic insights into precision epigenetic therapies.

## Methods
### Cell lines

HEK293T and PANC-1 cells were cultured in Dulbecco's Modified Eagle Medium (DMEM, Thermo fisher) with 10% fetal bovine serum (FBS, Adamas life) and 1% (v/v) penicillin-streptomycin solution (Beyotime). AsPC1 cells were cultured in RPMI-1640 medium which contained with 10% fetal bovine serum (FBS, Adamas life) and 1% (v/v) penicillin-

streptomycin solution (Beyotime). All cells were maintained at 37 °C in a humidified incubator containing 5% $CO_2$.

KDM5C[KO], KDM6A[KO] or KMT2B[KO] cells were generated by CRISPR/Cas9-mediated genome editing. The phenotype of knockout isolated clones was analyzed by western blots and their genotype was confirmed by Sanger DNA sequencing.

### RNA sequencing and quantitative real-time RT-PCR

Total RNA was extracted using Promega Total RNA Kit (Promega, LS1040) and quantified. Reverse transcription was performed using Reverse Transcriptase (Bioshare, SB-RT001) for cDNA synthesis. The sequencing library was prepared by Novogene company, and the RNA sequencing was performed on a Novaseq-PE150 (Novogene, Beijing).

Raw paired-end sequencing data were processed as follows: First, FastQC (v0.7.2) was employed to assess the quality of the sequences. Next, cutadapt (v5.0) was utilized to remove sequencing adapters and low-quality bases. The cleaned reads were then aligned to the human reference genome (hg38) using the STAR aligner (v2.7.11a) and annotated with the GENCODE v46. Raw read counts values were generated with featureCounts (v2.1.1). To identify differentially expressed genes (DEGs) between control and treatment conditions, raw RNA-seq count data were processed using the DESeq2 R package (v1.46.0) with the following statistical cutoff: | $\log_2FC$| > 0.585, FDR < 0.05.

RT-qPCR was carried out using 2×Universal SYBR Green qPCR Premix (Vazyme, Q312-02) on the CFX Opus96 RT-qPCR detection system (Bio-Rad), following the manufacturer's recommended procedures. Primers used for RT-qPCR are listed in Supplementary Data 5.

### GSEA analysis

All genes were first ranked based on expression patterns. Gene Set Enrichment Analysis (GSEA) was then conducted using the clusterProfiler R package (v 4.14.4), primarily focusing on Gene Ontology (GO) enrichment to identify key biological processes associated with the RNA-seq data.

### ATAC-seq library preparation and sequencing

ATAC-seq libraries were generated as previously described[51]. Briefly, 50,000 cells were collected at $500 \times g$ for 5 min, which was followed by a wash using 50 μl of cold 1×PBS and centrifugation at $500 \times g$ for 5 min. Cells were lysed using cold lysis buffer (10 mM Tris-HCl, pH 7.4, 10 mM NaCl, 3 mM $MgCl_2$ and 0.1% IGEPAL CA-630), then centrifuged for 10 min at $500 \times g$ to collect nuclei. Resuspend cell pellet in 50 ul of transposition mixture (25 μl 2 × TD buffer, 2.5 μl transposase (100 nM final), 16.5 μl PBS, 0.5 μl 1% digitonin, 0.5 μl 10% Tween-20, 5 μl H2O) by pipetting up and down 6 times. Incubate reaction at 37 °C for 30 min in a HUXImixer (HUXI, Shanghai) with 1000 RPM mixing. Transposition reactions were cleaned up with a UNIQ-10 Column MicroDNA Gel Extraction Kit (Songon Biotech, Shanghai). Libraries were amplified with Illumina Nextera sequencing primers in the same manner as previous[52]. Libraries were sequenced on a Novaseq-PE150 (Novogene, Beijing). Primers used for ATAC-seq are listed in Supplementary Data 5.

### ATAC-seq data analysis

Paired-end sequencing reads were processed using Cutadapt (v4.9) to remove adapter sequences and bases with quality scores below 30. Read quality was assessed before and after trimming using FastQC (v0.7.2). Trimmed reads were aligned to the human reference genome (hg38) using Bowtie2 (v2.5.3). Resulting BAM files were filtered with BAMTools (v2.5.2) to remove alignments with mapping quality (MAPQ) scores below 30 and reads mapped to the mitochondrial genome. PCR duplicates were subsequently removed using Picard MarkDuplicates (v3.1.1.0). Filtered BAM files were converted to BED format, and peak calling was performed using MACS2 (v2.2.9.1, parameters --shift -100 --extend 200). The adjusted p-value cut-off for peak detection was 0.05. For genomic annotation of ATAC-seq peaks, the ChIPseeker R package (v1.42.1) was applied, using the TxDb.Hsapiens.UCSC.hg38.knownGene database to associate peaks with

proximal genes. Promoters were defined as the 3000 bp region upstream of the transcription start site. BigWig files were generated using bamCoverage (--bin-50) from the deeptools (v3.5.4), with normalization to counts per million mapped reads. For genome-wide visualization, we utilized the Integrated Genome Browser (v2.19.1).

To identify differentially accessible regions (DARs) between HEK293T and other groups, we used the R package DiffBind (version 3.16.0). Data normalization was applied prior to analysis using the DBA_NORM_LIB method implemented in DiffBind. Differential accessibility analysis was then performed using the edgeR statistical method. The following criteria were applied to define significantly differentially accessible regions: | $\log_2$FC| > 0.263, FDR < 0.05.

The computematrix from deeptools(v3.5.4) was used in referencePoint "center" mode to calculate read enrichment in a 5000 bp window around the center of each region. Accessibility levels were visualized as heatmaps with the plotHeatmap function in deeptools.

### Identifying differentially accessible TF motifs using ATAC-seq data

For transcription factor motif prediction from ATAC-seq data, we extracted DNA sequences from the differentially accessible regions and performed motif enrichment analysis using the Automated Motif Extraction (AME) module in the MEME Suite (version 5.5.7). The JASPAR database was used for motif enrichment. Other parameters were set to default. The significance of the identified transcription factor motifs was assessed based on $p$ value, and only motifs with $p < 0.01$ were considered statistically significant.

### Direct binding profiling of TFs to target genes using ENCODE ChIP–seq datasets

Transcription factor (TF) target gene sets were curated from publicly available ChIP-seq datasets in the ENCODE Transcription Factor Targets Database (ENCODE Project Consortium, 2012) and Cistrome DB. Specifically, the following ENCODE datasets were used: ENCFF109ADF, ENCFF409YKQ, ENCFF303TSY, ENCSR747VUU, and ENCSR000BQX. Additionally, the dataset GSM501690 from Cistrome DB was integrated into the analysis. Peak files (BED format) were annotated using the ChIP-seeker R package. Peaks which overlapping promoter regions were retained, and their associated genes were compiled as candidate TF targets for downstream analysis.

### Proteomics of chromatin-binding proteins

Chromatin fractionation was performed following the previously described procedures[53]. The cells were lysed using a cytoplasmic lysis buffer (10 mM Tris-HCl, pH 8.0, 0.34 M sucrose, 3 mM $CaCl_2$, 2 mM $MgCl_2$, 0.1 mM EDTA, 1 mM DTT, 0.5% NP-40, protease inhibitor mixture) for 30 min on ice. The intact nuclei were subsequently collected by centrifugation at 5000 rpm for 2 min. The nuclear pellets were then homogenized in a nuclear lysis buffer (20 mM HEPES, pH 7.9, 1.5 mM $MgCl_2$, 1 mM EDTA, 150 mM KCl, 0.1% NP-40, 1 mM DTT, 10% glycerol, protease inhibitor mixture). After centrifugation at 14,000 rpm for 30 min, the chromatin-enriched pellet fraction was incubated in a chromatin isolation buffer, which contained 20 mM HEPES (pH 7.9), 1.5 mM $MgCl_2$, 150 mM KCl, 10% glycerol, protease inhibitor mixture and 0.15 unit/μl benzonase (Sigma), on ice for 2 h with gentle resuspension in every 10 min. After centrifugation at 5000 rpm for 2 min, the supernatant was collected as the chromatin fraction.

Protein digestion and peptide clean-up. Then the chromatin fraction proteins were digested, following a previously published protocol[54]. For each sample, 100 μg of protein were run in 10% SDS-PAGE gels until the dye front was 1 cm from the bottom for higher reproducibility. Dehydrated gel pieces were reduced with 10 mM dithiothreitol (DTT, Adamas, China) at 37 °C for 60 min, alkylated with 30 mM iodoacetamide (IAA) (Sigma-Aldrich, 16125-25G) in the dark at room temperature for 30 min, and digested with 2 ng/μl of trypsin (Thermo Fisher Scientific) in 25 mM NH4HCO3 overnight at 37 °C. Resulting peptide mixtures were cleaned

using Empore Stage Tips (6091, CDS Analytical, US) and dried using the SpeedVac Vacuum concentrator (ThermoFisher Scientific).

LC-MS/MS analyzes. The dried peptide samples were re-dissolved with 0.1% FA and further analyzed by electrospray liquid chromatography-tandem mass spectrometry using an Orbitrap Eclipse™ Tribrid™ coupled with Vanquish™ Neo UHPLC (Thermo Fisher Scientific). A total of 500 ng of samples were injected onto the peptide trap column and washed with a loading buffer (0.1% formic acid in water). The samples data were acquired using Data Independent Acquisition (DIA). DIA MS parameters were set to: (1) MS: scan range ($m/z$), 350–1500; orbitrap resolution, 60,000; ACG target, standard; cycle time (s), 3. (2) HCD-MS/MS: orbitrap resolution, 30,000; scan range ($m/z$), 200–2000, time (ms), 54; normalized AGC target (%), 1000; HCD CE (%), 32; 60 DIA isolation windows of 10 $m/z$ from $m/z$ 400–1000.

DIA data processing using DIANN. Raw DIA-MS datasets were processed using DIANN (version 1.8.1) in library-free mode with the following search settings: The analysis was performed in "Robust LC (high precision)" with precursor $m/z$ values ranging from 300 to 1800, fragment ion $m/z$ range from 200 to 1800, precursor charges between 1 and 4, trypsin with a maximum of 1 missed cleavage, peptide length range between 9 and 50 amino acids. Protein identities were assigned by searching against the in-silico tryptic digestion using the UniProt Homo sapiens reference database (UP000005640_9606, download December 9, 2024). Quantitative data analysis and visualization was performed using RStudio (version 4.3.1) within the R environment. The data was normalized using the DiaNN R package. The differentially expressed peptides and proteins were identified using the limma R package, with the following statistical cutoff: | $\log_2$FC| > 0.263, FDR < 0.05.

### Western blot

Samples for western blot were separation on a SDS-PAGE, the proteins were transferred to a 0.45 μm PVDF membrane (Millipore). After blocking with blotting-grade blocker (Bio-Rad), the membrane was incubated in a solution containing primary antibody and 5% BSA for 2 h at room temperature, and then incubated in a 5% blotting-grade blocker containing HRP-conjugated secondary antibody. The western blot signal was detected using ECL western blotting detection reagent (Bio-Rad, CFX Opus 96). Primary antibodies used in this study included histone H3 (Cell Signaling Technology, 9715S; 1:10,000), GAPDH (Share-bio, SB-AB0038; 1:5000), KDM5C (Abmart, TD13631; 1:1000), KDM6A (Abmart, TD13286; 1:1000), KMT2B (Abmart, TD8886; 1:1000), Anti-Histone H3 (tri methyl K4) antibody (Abcam, Ab8580; 1 μg/ml), Anti-Histone H3 (tri methyl K27) antibody (Abcam, Ab6002; 5 μg/ml).

### Virus preparation and transduction

Lentivirus were generated using psPAX2 and VSV-G packaging plasmids. For virus production, $5 \times 10^6$ HEK293T cells were plated into 10 cm dishes and transfected with the plasmids of interest using Lipo293™ (Beyotime, Shanghai, China) and appropriate packaging plasmids. Medium was changed 24 h later. Supernatants were collected at 48 h and 72 h, passed through 0.2 μm filters and applied at 50% concentration to target cells. 2 days after infection, cells were subjected to selected with Puromycin (2 μg/ml).

### Cell proliferation assay

Proliferation assay was performed by Cell Counting Kit-8 method. Briefly, the cells were seeded at a density of 2000 cells per well with 100 μl complete medium in 96-well cell culture plates, and incubated at 37 °C and humidified 5% $CO_2$. At 24 h, 48 h, 72 h, and 96 h after seeding, 10 μl CCK8 reagent (ShareBio, Shanghai, China) was added and incubated for 75 min at 37 °C. The absorbance values were then measured at a wavelength of 450 nm.

### Wound healing and transwell assays

Wound healing and transwell assays were performed as previously described[55]. Briefly, for the wound healing assay, the cells were plated in

6-well plates to form a full monolayer. A wound was created by scratching with a 200 µl pipette tip, and the intercellular distance was measured at 0 h, 24 h, 48 h, and 72 h.

For transwell invasion analysis, pretreated cells were cultured with 200 µl of serum-free DMEM medium in the upper chamber that had been loaded with or without Matrigel (BD biosciences, USA). The lower chamber was filled with 600 µl DMEM and 10% fetal bovine serum as chemoat-tractant. The cells were incubated for 24 h at 37 °C and 5% $CO_2$ and then non-migrated cells were removed from the top of the chamber with a cotton swab. The rest cells were fixed by absolute methanol, stained with Crystal Violet, and photographed using a microscope.

### Statistics and reproducibility
Two-tailed *t*-test was performed to compare two experimental groups. One-way ANOVA was used to determine whether three or four groups are statistically different from each other. For bioinformatic analyzes, as described in the Methods, chromatin proteomics data were analyzed for differential expression using the limma R package (v3.62.6), transcriptomic data were analyzed using DESeq2 (v1.46.0) with negative binomial tests, and ATAC-seq data underwent differential accessibility analysis using the DiffBind R package (v3.16.0). A two-sided Kolmogorov–Smirnov (KS) test was performed to calculate *p*-values by comparing the distribution of peaks associated with differentially expressed genes to those associated with all genes. Box plots were used to visualize the expression levels of transcription factor-regulated downstream genes. Differences in expression were assessed for statistical significance using paired *t*-tests, and *p*-values were calculated accordingly.

### Reporting summary
Further information on research design is available in the Nature Portfolio Reporting Summary linked to this article.

### Data availability
Raw ATAC-seq and RNA-seq sequencing data support the findings of this study have been deposited in the Gene Expression Omnibus (GEO) data-base under GSE295761 and GSE295762. Mass spectrometry data have been deposited to the ProteomeXchange Consortium (https://proteomecentral. proteomexchange.org) via the iProX partner repository[56] with the dataset identifier PXD063475. All relevant data generated and analyzed during this study can be found in Supplementary Information and in Supplementary Data1-6. All the other data supporting the findings of this study are available from the corresponding author upon reasonable request.

### Code availability
R scripts used for the bioinformatics analyses can be accessed at https:// github.com/archer2-34/code.git. Additionally, the code related to the ana-lysis described in this manuscript, along with the specific versions of the software tools detailed in the "Methods" section, has been archived in https://doi.org/10.5281/zenodo.17631089[57].

### References
1. Audia, J. E. & Campbell, R. M. Histone modifications and cancer. *Cold Spring Harb. Perspect. Biol.* **8**, a19521 (2016).
2. Zhao, S., Allis, C. D. & Wang, G. G. The language of chromatin modification in human cancers. *Nat. Rev. Cancer* **21**, 413–430 (2021).
3. Terekhanova, N. V. et al. Epigenetic regulation during cancer transitions across 11 tumour types. *Nature* **623**, 432–441 (2023).
4. Valencia, A. M. & Kadoch, C. Chromatin regulatory mechanisms and therapeutic opportunities in cancer. *Nat. Cell Biol.* **21**, 152–161 (2019).
5. Esteller, M. Cancer epigenomics: DNA methylomes and histone-modification maps. *Nat. Rev. Genet.* **8**, 286–298 (2007).
6. Zhao, Z. & Shilatifard, A. Epigenetic modifications of histones in cancer. *Genome Biol.* **20**, 245 (2019).
7. Wang, H. et al. H3k4me3 regulates RNA polymerase ii promoter-proximal pause-release. *Nature* **615**, 339–348 (2023).
8. Qu, Q. et al. Structure and conformational dynamics of a compass histone h3k4 methyltransferase complex. *Cell* **174**, 1117–1126 (2018).
9. Chen, K. et al. Broad h3k4me3 is associated with increased transcription elongation and enhancer activity at tumor-suppressor genes. *Nat. Genet.* **47**, 1149–1157 (2015).
10. Füllgrabe, J., Kavanagh, E. & Joseph, B. Histone onco-modifications. *Oncogene* **30**, 3391–3403 (2011).
11. Marsolier, J. et al. H3k27me3 conditions chemotolerance in triple-negative breast cancer. *Nat. Genet.* **54**, 459–468 (2022).
12. Ngollo, M. et al. The association between histone 3 lysine 27 trimethylation (h3k27me3) and prostate cancer: relationship with clinicopathological parameters. *BMC Cancer* **14**, 994 (2014).
13. Yagi, M. et al. Bivalent chromatin instructs lineage specification during hematopoiesis. *Cell* **188**, 4314–4331 (2025).
14. Liu, X. et al. Distinct features of h3k4me3 and h3k27me3 chromatin domains in pre-implantation embryos. *Nature* **537**, 558–562 (2016).
15. Timp, W. & Feinberg, A. P. Cancer as a dysregulated epigenome allowing cellular growth advantage at the expense of the host. *Nat. Rev. Cancer* **13**, 497–510 (2013).
16. Muntean, A. G. & Hess, J. L. Epigenetic dysregulation in cancer. *Am. J. Pathol.* **175**, 1353–1361 (2009).
17. Castro-Muñoz, L. J. et al. Modulating epigenetic modifications for cancer therapy. *Oncol. Rep.* **49**, 59 (2023).
18. Mohammad, H. P., Barbash, O. & Creasy, C. L. Targeting epigenetic modifications in cancer therapy: erasing the roadmap to cancer. *Nat. Med.* **25**, 403–418 (2019).
19. Hogg, S. J., Beavis, P. A., Dawson, M. A. & Johnstone, R. W. Targeting the epigenetic regulation of antitumour immunity. *Nat. Rev. Drug Discov.* **19**, 776–800 (2020).
20. Da Silva Santos, M. E. et al. Kmt2 (mll) family of methyltransferases in head and neck squamous cell carcinoma: a systematic review. *Head. Neck* **46**, 417–434 (2024).
21. Hao, F. Systemic profiling of kdm5 subfamily signature in non-small-cell lung cancer. *Int. J. Gen. Med.* **14**, 7259–7275 (2021).
22. Hoffmann, M. J. & Schulz, W. A. Alterations of chromatin regulators in the pathogenesis of urinary bladder urothelial carcinoma. *Cancers* **13**, 6040 (2021).
23. Huang, H. et al. Multi-omics analyses reveal spatial heterogeneity in primary and metastatic oesophageal squamous cell carcinoma. *Clin. Transl. Med.* **13**, e1493 (2023).
24. Garcia-Recio, S. et al. Multiomics in primary and metastatic breast tumors from the aurora us network finds microenvironment and epigenetic drivers of metastasis. *Nat. Cancer* **4**, 128–147 (2022).
25. Cai, W. L. et al. Specific chromatin landscapes and transcription factors couple breast cancer subtype with metastatic relapse to lung or brain. *BMC Med. Genomics* **13**, 1–18 (2020).
26. Xue, Y. et al. Unraveling the key role of chromatin structure in cancer development through epigenetic landscape characterization of oral cancer. *Mol. Cancer* **23**, 190 (2024).
27. Kandoth, C. et al. Mutational landscape and significance across 12 major cancer types. *Nature* **502**, 333–339 (2013).
28. Martínez-Jiménez, F. et al. A compendium of mutational cancer driver genes. *Nat. Rev. Cancer* **20**, 555–572 (2020).
29. Timothy, L. et al. The meme suite. *Nucleic Acids Res.* **43**, W39–W49 (2015).
30. Orzechowska-Licari, E. J., Lacomb, J. F., Mojumdar, A. & Bialkowska, A. B. Sp and klf transcription factors in cancer metabolism. *Int. J. Mol. Sci.* **23**, 9956 (2022).
31. Safe, S. & Abdelrahim, M. Sp transcription factor family and its role in cancer. *Eur. J. Cancer* **41**, 2438–2448 (2005).

32. Bowman, T., Garcia, R., Turkson, J. & Jove, R. Stats in oncogenesis. *Oncogene* **19**, 2474–2488 (2000).
33. Millán-Zambrano, G., Burton, A., Bannister, A. J. & Schneider, R. Histone post-translational modifications — cause and consequence of genome function. *Nat. Rev. Genet.* **23**, 563–580 (2022).
34. Lukauskas, S. et al. Decoding chromatin states by proteomic profiling of nucleosome readers. *Nature* **627**, 671–679 (2024).
35. Husmann, D. & Gozani, O. Histone lysine methyltransferases in biology and disease. *Nat. Struct. Mol. Biol.* **26**, 880–889 (2019).
36. van Dam, H. & Castellazzi, M. Distinct roles of jun: fos and jun: atf dimers in oncogenesis. *Oncogene* **20**, 2453–2464 (2001).
37. Shah, N. & Sukumar, S. The hox genes and their roles in oncogenesis. *Nat. Rev. Cancer* **10**, 361–371 (2010).
38. Mazor, G. et al. The lncrna tp73-as1 is linked to aggressiveness in glioblastoma and promotes temozolomide resistance in glioblastoma cancer stem cells. *Cell Death Dis.* **10**, 246 (2019).
39. Rodriguez-Bravo, V. et al. The role of gata2 in lethal prostate cancer aggressiveness. *Nat. Rev. Urol.* **14**, 38–48 (2017).
40. Yunhai, L. et al. New developments on the encyclopedia of dna elements (encode) data portal. *Nucleic Acids Res.* **48**, D882–D889 (2019).
41. Mrozik, K. M., Blaschuk, O. W., Cheong, C. M., Zannettino, A. & Vandyke, K. N-cadherin in cancer metastasis, its emerging role in haematological malignancies and potential as a therapeutic target in cancer. *BMC Cancer* **18**, 939 (2018).
42. Gouin, K. R. et al. An n-cadherin 2 expressing epithelial cell subpopulation predicts response to surgery, chemotherapy and immunotherapy in bladder cancer. *Nat. Commun.* **12**, 4906 (2021).
43. Li, L. et al. Klf4-mediated cdh3 upregulation suppresses human hepatoma cell growth and migration via gsk-3β signaling. *Int. J. Biol. Sci.* **15**, 953–961 (2019).
44. Mizrahi, J. D., Surana, R., Valle, J. W. & Shroff, R. T. Pancreatic cancer. *Lancet* **395**, 2008–2020 (2020).
45. Bailey, P. et al. Genomic analyses identify molecular subtypes of pancreatic cancer. *Nature* **531**, 47–52 (2016).
46. Leng, X. et al. Histone 3 lysine-27 demethylase kdm6a coordinates with kmt2b to play an oncogenic role in nsclc by regulating h3k4me3. *Oncogene* **39**, 6468–6479 (2020).
47. Seehawer, M. et al. Loss of kmt2c or kmt2d drives brain metastasis via kdm6a-dependent upregulation of mmp3. *Nat. Cell Biol.* **26**, 1165–1175 (2024).
48. Bai, J. et al. Satb1 in cancer progression and metastasis: mechanisms and therapeutic potential. *Front. Oncol.* **15**, 1535929 (2025).
49. Nguyen, H. T. & Martin, L. J. Classical cadherins in the testis: how are they regulated? *Reprod. Fertil. Dev.* **35**, 641–660 (2023).
50. Gao, J., Yan, Q., Wang, J., Liu, S. & Yang, X. Epithelial-to-mesenchymal transition induced by tgf-β1 is mediated by ap1-dependent epcam expression in mcf-7 cells. *J. Cell. Physiol.* **230**, 775–782 (2015).
51. Corces, M. R. et al. An improved atac-seq protocol reduces background and enables interrogation of frozen tissues. *Nat. Methods* **14**, 959–962 (2017).
52. Buenrostro, J. D., Wu, B., Chang, H. Y. & Greenleaf, W. J. Atac-seq: a method for assaying chromatin accessibility genome-wide. *Curr. Protoc. Mol. Biol.* **109**, 21–29 (2015).
53. Li, L., Miao, W., Huang, M., Williams, P. & Wang, Y. Integrated genomic and proteomic analyses reveal novel mechanisms of the methyltransferase setd2 in renal cell carcinoma development. *Mol. Cell. Proteom.* **18**, 437–447 (2019).
54. Bing, T., Shangguan, D. & Wang, Y. Facile discovery of cell-surface protein targets of cancer cell aptamers. *Mol. Cell. Proteom.* **14**, 2692–2700 (2015).
55. Liu, L. et al. Kdm6a-arhgdib axis blocks metastasis of bladder cancer by inhibiting Rac1. *Mol. Cancer* **20**, 77 (2021).
56. Tao, C. et al. Iprox in 2021: connecting proteomics data sharing with big data. *Nucleic Acids Res.* **50**, D1522–D1527 (2021).
57. Li, T. & Wang, L. Multi-omics elucidation of KDM5C, KDM6A, and KMT2B roles in cancer epigenetic dysregulation and transcriptional reprogramming. Zenodo. https://doi.org/10.5281/zenodo.17631089 (2025).

## Acknowledgements

## Author contributions

T.L. and L.L. conceived the study and designed the experiment. T.L., L.W., S.D., and X.C. performed all the experiments. T.L., L.W., C.F., and J.H. performed the data analyses. T.L. and L.L. drafted the manuscript. All the authors discussed the results and commented on the manuscript. Project administration and funding acquisition: L.L.

## Competing interests

The authors declare no competing interests.

## Additional information

**Supplementary information** The online version contains supplementary material available at https://doi.org/10.1038/s42003-025-09305-z.

**Correspondence** and requests for materials should be addressed to Lin Li.

**Peer review information** *Communications Biology* thanks Gianluca Sigismondo and the other, anonymous, reviewer(s) for their contribution to the peer review of this work. Primary Handling Editors: Silvia Belluti and Johannes Stortz. A peer review file is available.

**Reprints and permissions information** is available at http://www.nature.com/reprints

**Publisher's note** Springer Nature remains neutral with regard to jurisdictional claims in published maps and institutional affiliations.